On the Importance of Vaisala RS92 Radiosonde Humidity Corrections for a Better Agreement between Measured and Modeled Satellite Radiances

AJIL KOTTAYIL AND STEFAN A. BUEHLER

SRT–RY, Luleå University of Technology, Kiruna, Sweden

VIJU O. JOHN

Met Office Hadley Centre, Exeter, United Kingdom

LARRY M. MILOSHEVICH

Milo Scientific LLC, Lafayette, Colorado

M. MILZ AND G. HOLL

SRT–RY, Luleå University of Technology, Kiruna, Sweden

(Manuscript received 5 May 2011, in final form 31 October 2011)

ABSTRACT

A study has been carried out to assess the importance of radiosonde corrections in improving the agreement between satellite and radiosonde measurements of upper-tropospheric humidity. Infrared [High Resolution Infrared Radiation Sounder (HIRS)-12] and microwave [Advanced Microwave Sounding Unit (AMSU)-18] measurements from the *NOAA-17* satellite were used for this purpose. The agreement was assessed by comparing the satellite measurements against simulated measurements using collocated radiosonde profiles of the Atmospheric Radiation Measurement (ARM) Program undertaken at tropical and midlatitude sites. The Atmospheric Radiative Transfer Simulator (ARTS) was used to simulate the satellite radiances. The comparisons have been done under clear-sky conditions, separately for daytime and nighttime soundings. Only Vaisala RS92 radiosonde sensors were used and an empirical correction (EC) was applied to the radiosonde measurements. The EC includes correction for mean calibration bias and for solar radiation error, and it removes radiosonde bias relative to three instruments of known accuracy. For the nighttime dataset, the EC significantly reduces the bias from 0.63 to −0.10 K in AMSU-18 and from 1.26 to 0.35 K in HIRS-12. The EC has an even greater impact on the daytime dataset with a bias reduction from 2.38 to 0.28 K in AMSU-18 and from 2.51 to 0.59 K in HIRS-12. The present study promises a more accurate approach in future radiosonde-based studies in the upper troposphere.

1. Introduction

The vertical distribution of water vapor in the troposphere is quite inhomogeneous, ranging from concentrations of a few percent near the surface to only a few parts per million near the tropopause. Despite the fact that the upper-tropospheric water vapor constitutes only a small fraction of the total water vapor, it still has a large effect on the outgoing longwave radiation (Kiehl and Briegleb 1992). Model studies suggest that nearly two-thirds of the total radiative feedback from water vapor occurs in the upper troposphere (Held and Soden 2000). These studies confirm the need for an accurate monitoring of the upper-tropospheric humidity (UTH), which is not very well simulated in current climate models (John and Soden 2007). One of the sources of UTH measurements is radiosonde data since the mid-twentieth century. These observations, however, are limited mainly to land areas and are known to have data quality issues (Elliott and Gaffen 1991; Miloshevich et al. 2009; Soden and Lanzante 1996).

Corresponding author address: Ajil Kottayil, Division of Space Technology, Department of Computer Science, Electrical and Space Engineering, Luleå University of Technology, Box 812, SE-98128 Kiruna, Sweden.
E-mail: ajil.kottayil@ltu.se

DOI: 10.1175/JTECH-D-11-00080.1

The satellite era has offered us the advantage of measuring UTH globally, along with a wealth of other information to understand the earth's atmospheric system better. In the microwave and infrared spectral range, certain frequency ranges are dominated by water vapor emission from a broad range of pressure levels approximately between 200 and 500 hPa. These frequency ranges are suitable for deriving UTH. The typical frequencies used for this application are 6.7 μm for infrared and 183 $\pm$ 1 GHz for microwave. The term UTH was first used by Soden and Bretherton (1993), to describe relative humidity regressed from satellite-observed brightness temperatures obtained by broadband infrared instruments. A similar approach was followed by Buehler and John (2005) to derive UTH from microwave measurements near the 183-GHz water vapor emission line.

Although there have been studies on both infrared and microwave measurements (Buehler et al. 2004; Soden and Lanzante 1996), none of the studies thus far have looked into both instrument types simultaneously to judge their consistency. For this purpose, the satellite infrared and microwave measurements have been collocated with radiosonde profiles of the Atmospheric Radiation Measurements (ARM) Program undertaken at midlatitude and tropical locations. The comparisons were performed in radiance space by simulating the infrared and microwave channel radiance from the radiosonde data using the Atmospheric Radiative Transfer Simulator (ARTS; Eriksson et al. 2011).

The relative humidity (RH) measurements from Vaisala radiosondes are known to have a dry bias in the upper troposphere (Vömel et al. 2007b; Moradi et al. 2010). Recently, Miloshevich et al. (2009) have implemented an empirical correction procedure to remove the mean bias error in RS92 radiosonde sensors by characterizing their accuracy relative to three reference instruments of known accuracy. We have applied this correction to the RS92 radiosonde profiles. The correction is applied for mean calibration bias as a function of RH and temperature. A correction for solar radiation error resulting from solar heating of the RH sensor is also applied for daytime soundings. In addition, a nonbias correction for sensor time lag (TL) error caused by slow response at low temperature is also examined. The TL correction recovers vertical structure in the RH profile that was ''smoothed'' by slow sensor response (Miloshevich et al. 2004). Although the time lag correction is not directly a bias correction, it may remove some parts of a bias, in particular, in regions with strong gradients. An important objective of this study is to assess whether the various corrections improve the agreement between the radiosonde and satellite data in both the infrared and microwave bands.

The paper is structured as follows: Section 2 focuses on the details of measurements and the models and methods used. Section 3 presents results and discussions on the impact of radiosonde correction procedure in satellite–radiosonde comparison. Finally, section 4 presents the summary and conclusions.

2. Measurements, models, and methods used

a. Satellite data

The *National Oceanic and Atmospheric Administration* (*NOAA*)*-17* satellite carries the Advanced Microwave Sounding Unit (AMSU) and the High Resolution Infrared Sounder (HIRS)-3. AMSU consists of AMSU-A and AMSU-B sensors, with a total of 20 channels. The primary function of the 15-channel AMSU-A (channels 1–15) is to provide temperature sounding of the atmosphere. The five channels of AMSU-B (channels 16–20) mainly measure water vapor and liquid precipitation over land and sea. Three channels (18–20) are situated around the strong water vapor spectral line at 183.31 GHz with different offsets from the line center. AMSU-B is a cross-track, continuous line scanning, total power radiometer with an instantaneous field of view of 1.18° (at the half-power points), equivalent to a nominal spatial resolution of 16 km at nadir. The antenna provides a cross-track scan, scanning $\pm$49.5° from nadir with a total of 90 Earth fields of view per scan line.

HIRS-3 on board *NOAA-17* is a 20-channel instrument with an instantaneous field of view of 1.38°, providing a nominal spatial resolution of 18.9 km at nadir. The antenna provides a cross-track stepped scan covering $\pm$49.58° from nadir with a total of 56 fields of view per scan. The spectral characteristics of the HIRS-3 channels are available online (see http://www.ncdc.noaa.gov/oa/pod-guide/ncdc/docs/klm/index.htm). The spectral characteristics differ between different satellites. Hereafter, the two channels used in inferring UTH measurements, namely, HIRS channel 12 and AMSU channel 18, will be referred to as HIRS-12 (6.7 μm) and AMSU-18 (183 $\pm$ 1 GHz; Soden and Bretherton 1993; Buehler and John 2005; Buehler et al. 2008). We have used measurements of HIRS-12 and AMSU-18 for the period of 2005–08 on *NOAA-17*.

b. Radiosonde data and the correction methods

The ARM program operated by the U.S. Department of Energy launches radiosondes from several dedicated sites. We have used radiosonde data from 2005 to 2008 of two stations: one in the Southern Great Plains (SGP) at 36.61°N, 97.49°W in the United States, and one in the tropical western Pacific, located at 12.42°S, 130.88°E

near Darwin, on the northwestern coast of Australia. We have taken day- and nighttime radiosonde data measured using Vaisala RS92 sensors. The number of profiles used for nighttime analysis is 624 out of which 457 belong to SGP and 167 belong to Darwin. All of the 419 profiles used for daytime analysis belong to SGP. The profiles used to study the impact of the time lag correction also belong to SGP.

The accuracy of radiosonde RH measurements in the upper troposphere is known to be poor. A number of studies have shown that RS92 radiosonde sensors exhibit a dry bias in the upper troposphere (Vömel et al. 2007b; Moradi et al. 2010). Miloshevich et al. (2009) have characterized the accuracy of RS92 RH sensors relative to three water vapor reference instruments of known accuracy. The reference instruments are a cryogenic frost-point hygrometer (CFH; Vömel et al. 2007a), which quantifies the accuracy of RS92 above 700 mb; a microwave radiometer, which mainly senses water vapor in the lower troposphere; and a system of six calibrated RH probes at the surface. The RS92 mean calibration bias was determined by comparing RS92 measurements with simultaneous measurements from these instruments, and an empirical correction (EC) procedure was described that removes the RS92 mean bias as a function of RH and pressure P,

$$\mathrm{RH}_{\mathrm{corr}} = G(P, \mathrm{RH}) \times \mathrm{RH}, \quad (1)$$

where $G(P, \mathrm{RH})$ is the correction factor. The correction factor is determined from the pressure-dependent curve fits for several RH intervals (Fig. 9 in Miloshevich et al. 2009), with different curve fits for nighttime and daytime soundings. The bias error that is corrected for nighttime soundings is the mean sensor calibration bias. The daytime soundings are additionally affected by an error caused by solar heating of the RH sensor. Therefore, in addition to the mean sensor calibration bias correction, the daytime soundings also require a correction to remove the bias resulting from the so-called solar radiation error (SRE). Hence, the bias and the correction for daytime soundings would be higher than the nighttime soundings. In presence of clouds the daytime corrections could, in fact, overcorrect the radiation bias. However, this is not a factor in this study because only clear conditions were used. We have applied these corrections on RS92 radiosonde data and quantified their effect by comparing the corrected data to satellite measurements.

This study uses a modified version of the published correction for mean calibration bias that improves the accuracy for very dry conditions, and extends the upper limit of validity of the correction to encompass the tropical upper troposphere/lower stratosphere (UT/LS). The primary difference is that the correction was converted from a function of pressure to a function of temperature based on the mean $T(P)$ relationship for the soundings used to derive the correction. Temperature dependence is more consistent with the actual sensor calibration and generalizes the correction to atmospheric profiles substantially differently from the midlatitude soundings used to derive the correction. Additional details of the modified correction for mean calibration bias and associated IDL code can be found online (http://milo-scientific.com/prof/radiosonde.php).

The correction procedure described by Miloshevich et al. (2009) also includes a correction for sensor time-lag error that causes ''smoothing'' of the measured RH profile resulting from a slow sensor response at low temperatures. To see whether the time-lag correction has a significant role in reducing the brightness temperature bias, a subset of RS92 profiles was also corrected for time-lag error as described by Miloshevich et al. (2004). A subset of soundings is used because older ARM data (and most operational RS92 data) have integer RH values, which result in a less accurate time-lag correction because much of the detailed information important for a time-lag correction is lost due to ''rounding off'' of the data. For this and other reasons, it is recommended that users of the Vaisala Digicora III data system output the higher-resolution RH data in so-called Floating-Point Electronic Data Transfer (FLEDT) files rather than the integer RH values in standard Electronic Data Transfer (EDT) files.

It should be noted here that in December 2010, Vaisala updated their data-processing algorithm to include time-lag and solar radiation corrections that differ from those of Miloshevich et al. (2009), but this does not include the correction for the mean calibration bias used in this study. This change affects only new Digicora III data systems or older systems updated with software version 3.64, and the effect on soundings is described in Vaisala's ''RS92 data continuity'' website.

c. *Radiative transfer model*

The ARTS is a line-by-line radiative transfer model that simulates radiances from the infrared to the microwave spectral range (Buehler et al. 2005; Eriksson et al. 2011). The model uses precalculated absorption data to speed up the calculation, as described in Eriksson et al. (2011).

The code is flexible from the user's point of view and is freely available, along with comprehensive documentation (http://www.sat.ltu.se/arts/). The ARTS model has been validated against other models and satellite measurements (John and Buehler 2005; Melsheimer et al. 2005; Saunders et al. 2007). The model has been used for a wide range of atmospheric studies, including

applications from the infrared to the microwave wavelength range (Deuber et al. 2005; Fiorucci et al. 2008; Eriksson et al. 2003).

Buehler et al. (2010) recently implemented a fast setup to reduce the computational cost of the broadband radiance simulations of HIRS channels through the representative frequency selection by simulated annealing. The computational cost has been reduced significantly while keeping the accuracy of the radiance calculations the same as the conventional line-by-line calculations. They have shown that the HIRS channel radiances on *NOAA-14* can be simulated with only 133 frequencies. For comparison, a full line-by-line calculation would require 72 717 frequencies. The accuracy of this method is of the order of 0.03 K. This modified setup has been used for the present study.

Different continuum models have to be used for the infrared and the microwave spectral range. The absorption model setups for the two different spectral ranges are as follows. In the microwave, we have used PWR98 (Rosenkranz 1998) for H_2O lines and continuum and PWR93 (Rosenkranz 1993) for N_2 and O_2 lines and their respective continua. Furthermore, line data of O_3 was taken from the High Resolution Transmission (HITRAN) 2004 database (Rothman et al. 2003). In the infrared, line data were taken from HITRAN 2004 while the continua of H_2O, CH_4, N_2, O_2, and CO_2 were taken from MT_CKD_1.0 (Mlawer et al. 2003). A model intercomparison study between ARTS and the LBLRTM, an established reference model for the infrared spectral range was carried out for HIRS-12 on *NOAA-14, -15, -16* and *-17* satellites. The model comparison approach is described in the appendix. The two RT models were found to agree within a brightness temperature difference of 0.22 K. ARTS includes various algorithms to simulate the influence of clouds (Davis et al. 2005; Emde et al. 2004). However, for the present study only clear-sky simulations were performed.

d. Collocations and cloud detection approach

The collocations between *NOAA-17* measurements and ARM radiosondes are based on spatial and temporal constraints. The spatial constraint is implemented by a target area of a 50-km radius around the radiosonde location, as in Buehler et al. (2004). This approximately takes into account the drift of the radiosonde as it ascends through the atmosphere. The number of collocated pixels in a target area varies from 2 to 8 for HIRS-12 and from 10 to 30 for AMSU-18, respectively. The time constraint imposed on the collocated dataset is ±2 h. This should accommodate the time taken for the radiosonde to reach the satellite-measuring altitude peak (300 hPa), which is approximately 25 min. Hence, the radiosonde time in the collocated dataset is the sum of the radiosonde launch time and 25 min. Radiances are simulated from radiosonde profiles using ARTS to match with the satellite-viewing geometry.

A meaningful comparison between satellite measurements and clear-sky RT model simulations is possible only if the measurements are free of cloud contamination. Therefore, we use the cloud detection tests developed by McMillin and Dean (1982) to filter out contaminated HIRS pixels from our analysis. Details of this procedure are as follows:

Each pixel from satellite measurements is subjected to the following cloud detection tests. The first two tests are based on the longwave window channel (11 μm) brightness temperature and are applicable to all of the measurements:

(i) A pixel is classified as cloudy if its window channel brightness temperature is too cold (<210 K).
(ii) A pixel is classified as cloudy, if the longwave window channel brightness temperature is 4 K cooler than that of the warmest pixel from the target area.
(iii) If any one of the followings conditions fail for nighttime measurements, then the pixel is classified as cloudy:

$$-4.0\ \text{K} \le \text{TB}(18) - \text{TB}(8) \le 2.0\ \text{K},$$

$$-4.0\text{K} \le \text{TB}(19) - \text{TB}(18) \le 2.0\ \text{K}.$$

(iv) During the day a pixel is clear if

$$|\text{TB}(18) - \text{TB}(8)| < 10\ \text{K},$$

where TB(i) is the brightness temperature for a given HIRS channel i. If there is more than one clear pixel in the target area, the average over all the clear pixels are used; otherwise, it is classified as cloudy. This very stringent clear scene requirement condition satisfies 25%–100% of the target area for HIRS depending on the cloud cover. We assume that the AMSU-18 pixels coincident to the clear HIRS-12 pixels are not cloud contaminated. This could even result in the removal of the AMSU-18 pixels, which are unaffected by clouds because of the much higher sensitivity of HIRS measurements to thin clouds.

e. Relation between UTH and brightness temperature

The relationship between UTH and brightness temperature TB is given by

$$\ln(\text{UTH}) = a + b \times \text{TB}, \tag{2}$$

TABLE 1. The regression coefficients a and b used to derive UTH from HIRS-12 for its different viewing angles. The UTH is defined with respect to liquid water.

θ (°)	a (Dimensionless)	b (K^{-1})
0.900	29.554	−0.110
2.700	29.556	−0.110
4.500	29.560	−0.110
6.300	29.566	−0.110
8.100	29.574	−0.110
9.900	29.584	−0.110
11.700	29.596	−0.110
13.500	29.610	−0.110
15.300	29.626	−0.111
17.100	29.645	−0.111
18.900	29.667	−0.111
20.700	29.691	−0.111
22.500	29.718	−0.111
24.300	29.748	−0.111
26.100	29.781	−0.112
27.900	29.818	−0.112
29.700	29.859	−0.112
31.500	29.904	−0.112
33.300	29.955	−0.113
35.100	30.011	−0.113
36.900	30.073	−0.113
38.700	30.143	−0.114
40.500	30.222	−0.114
42.300	30.311	−0.115
44.100	30.412	−0.116
45.900	30.529	−0.116
47.700	30.666	−0.117
49.500	30.828	−0.118

where a and b can be determined by linear regression. The derivative yields

$$\frac{\Delta \mathrm{UTH}}{\mathrm{UTH}} = b \times \Delta T. \tag{3}$$

In other words, absolute changes in brightness temperature map to relative changes in UTH. To ensure complete consistency here, we have redetermined the parameters $b_{\mathrm{HIRS\_12}}$ and $b_{\mathrm{AMSU\_18}}$ using linear regression on the simulated measurements for the Chevallier et al. (2006) dataset. The values obtained for $b_{\mathrm{HIRS\_12}}$ and $b_{\mathrm{AMSU\_18}}$ are 0.110 and 0.070 for the nadir-viewing direction. For the extreme off-nadir viewing direction the $b_{\mathrm{HIRS\_12}}$ and $b_{\mathrm{AMSU\_18}}$ values are 0.118 and 0.076. These values are in good agreement with Soden and Bretherton (1993) and Buehler and John (2005). The regression coefficients a and b for different viewing angles of HIRS-12 are summarized in Table 1.

f. Ozone impact on AMSU-18 radiances

The impact of ozone lines on AMSU-B radiances was investigated by John and Buehler (2004). They found that the ozone impact is largest for AMSU-18. This can reduce its brightness temperature, with a reduction that can reach a maximum of 0.5 K. It was also reported that zonal, monthly mean climatological values of ozone profiles are sufficient to account for the ozone impact on AMSU-18 radiances. With the above work as a base, temperature and humidity profiles from ARM radiosondes were taken up to 100 hPa, and the rest of the pressure levels up to 0.2 hPa were filled in with climatological ozone and temperature profiles for AMSU-18 simulations. A water vapor concentration of 5 ppmv was assumed above 100 hPa. It is to be noted that the temperature and humidity profiles above 100 hPa have negligible impact on the AMSU-18 radiance. Thus, it is the presence of ozone that contributes to the impact. Climatological ozone and temperature profiles from Total Ozone Mapping Spectrometer (TOMS) version (v8), which are given for each 10° latitude bin and month, were used to fill in the radiosondes above 100 hPa. In the case of the HIRS-12 simulations, we have restricted the temperature and humidity profiles from ARM radiosondes to 90 hPa because the profiles above this level have negligible impact on HIRS-12 radiances. Ozone has no influence on HIRS-12 simulations.

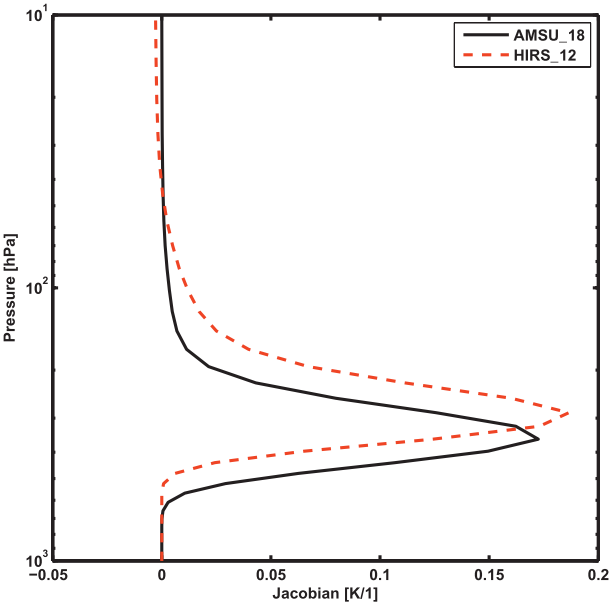

FIG. 1. Jacobian of AMSU-18 and HIRS-12 UTH channels for the standard tropical atmosphere (Garand et al. 2001) with a nadir viewing geometry. Jacobian values are divided by their sum.

3. Results and discussion

The radiosonde–satellite comparison results in terms of bias for AMSU-18 and HIRS-12 are discussed in this section. The results of daytime and nighttime comparisons

TABLE 2. Statistics comparing satellite radiance and simulated radiance in brightness temperature units for the nighttime dataset. The bias is defined as the mean of simulated minus measured data. SD refers to the standard deviation. The number of profiles used is 624. Suffixes bc and ac refers to before and after empirical correction.

Channel	Bias (K)	Bias in UTH (%)	SD (K)	SD UTH (%)
AMSU-18$_{bc}$	0.63	−4.5	1.66	11.62
AMSU-18$_{ac}$	−0.10	0.7	1.68	11.76
HIRS-12$_{bc}$	1.26	−14.3	1.40	16
HIRS-12$_{ac}$	0.35	−3.9	1.42	16.18

are presented separately. The bias is calculated as the mean of the difference between the simulated and measured brightness temperature, so a positive bias means that the radiosonde measurements are dry and vice versa. The same convention is followed throughout the discussion that follows.

The bias value can be used to determine the relative difference in the UTH measurements between the satellite and radiosonde. Applying the transformation coefficients [b_{HIRS_12}(0.114) and b_{AMSU_18} (0.073)] in Eq. (3), it can be inferred that a 1-K bias in AMSU-18 corresponds to a relative error of 7% in UTH, whereas for HIRS-12 it corresponds to a relative difference of 11%. Even though both AMSU-18 and HIRS-12 measure UTH, their sensitivity lies at slightly different altitudes. As shown in Fig. 1, the peak of HIRS-12 sensitivity lies approximately 2 km higher in altitude than for AMSU-18. These differences in sensing height will lead to a bias rather than a random error. Knowing the fact that radiosonde bias is altitude dependent (Miloshevich et al. 2009), the bias for HIRS-12 and AMSU-18 could be different because the sounding altitudes of the two instruments are not the same.

As a separate study to show the impact of ozone in AMSU-18 simulations, we have calculated the bias with and without the inclusion of ozone. The nighttime-uncorrected

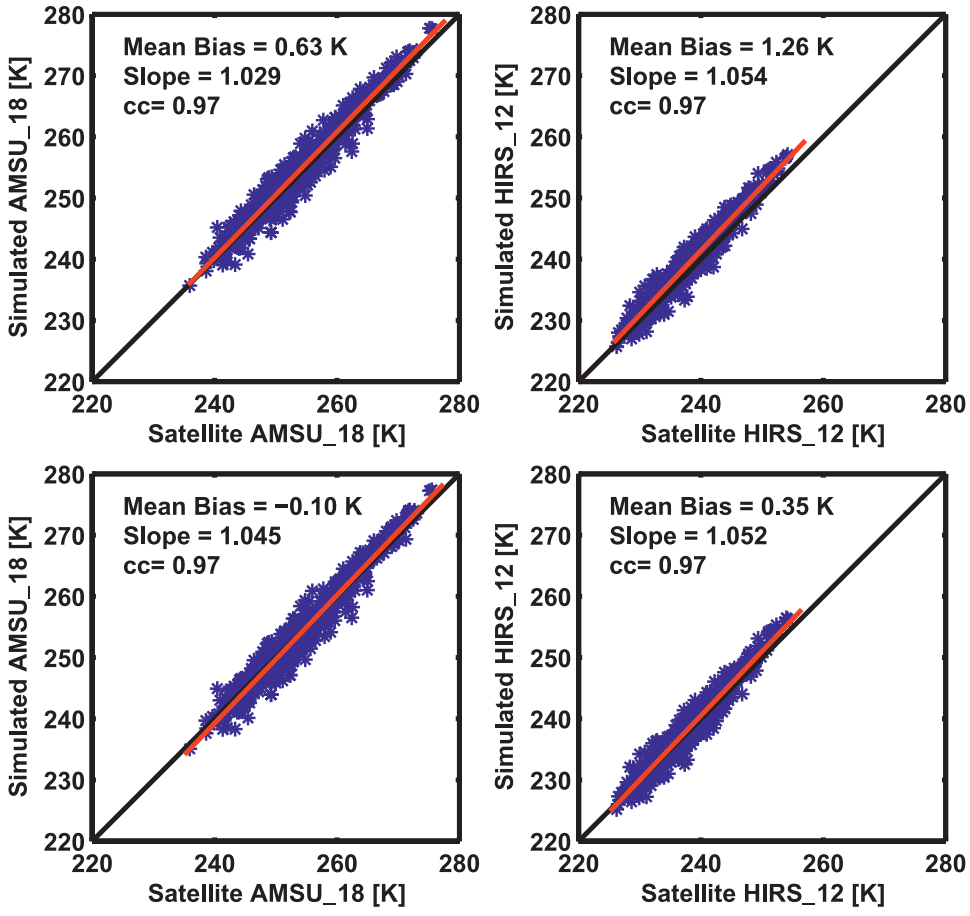

FIG. 2. Scatterplots of simulated vs observed brightness temperature for AMSU-18 and HIRS-12 (top) before and (bottom) after empirical correction (corrected RS92) for the nighttime data. Diagonal (black) and regression (red) lines are shown. The number of data points is 624 for each plot.

TABLE 3. Statistics comparing satellite radiance and simulated radiance in brightness temperature units for the daytime dataset. The bias is defined as the mean of simulated minus measured data. SD refers to the standard deviation. The number of profiles used is 419. Suffixes bc and ac refers to before and after empirical correction.

Channel	Bias (K)	Bias in UTH (%)	SD (K)	SD UTH (%)
AMSU-18_{bc}	2.38	−16.6	1.31	9.17
AMSU-18_{ac}	0.28	−1.96	1.39	9.73
HIRS-12_{bc}	2.51	−28.61	1.19	13.57
HIRS-12_{ac}	0.59	−6.73	1.27	14.48

radiosonde datasets were alone chosen for this study. The results reveal that the inclusion of ozone improved the bias to 0.63 K from a bias of 0.99 K. Obviously, here the inclusion of ozone reduces the AMSU-18 brightness temperature by 0.35 K. This is a clear confirmation that inclusion of ozone leads to a better agreement between satellite- and radiosonde-measured UTH as argued by John and Buehler (2004).

The nighttime comparison results for AMSU-18 and HIRS-12 are summarized in Table 2. Also, Fig. 2 shows a scatterplot of simulated versus observed brightness temperatures for AMSU-18 and HIRS-12 before and after correction. The empirical correction reduces the bias from 0.63 to −0.1 K for AMSU-18 and from 1.26 to 0.35 K for HIRS-12. The reduction in the bias is higher for HIRS-12 (0.91 K) in comparison to AMSU-18 (0.73 K). The results of daytime analysis are presented in Table 3. In contrast to the nighttime biases, the daytime biases in the uncorrected datasets are much higher (2.38 K in AMSU-18 and 2.51 K in HIRS-12). As a result, the empirical correction on daytime datasets has a profound influence in reducing the bias in AMSU-18 and HIRS-12. Accordingly, the bias reduction is of the order of 2.1 K for AMSU-18 and 1.92 K for HIRS-12. This clearly is an indication that the corrections are especially required for all daytime radiosonde observations, which are subject to solar radiation error. Recall that in addition to the mean bias correction as applied in the nighttime dataset, the daytime correction also includes a correction for solar radiation error, which is most significant here.

The bias as a function of brightness temperature binned at 5-K intervals for the day- and nighttime datasets is shown in Fig. 3. The reduction in bias resulting from correction is evident in all brightness temperature ranges, which represent varying humidity conditions in the upper

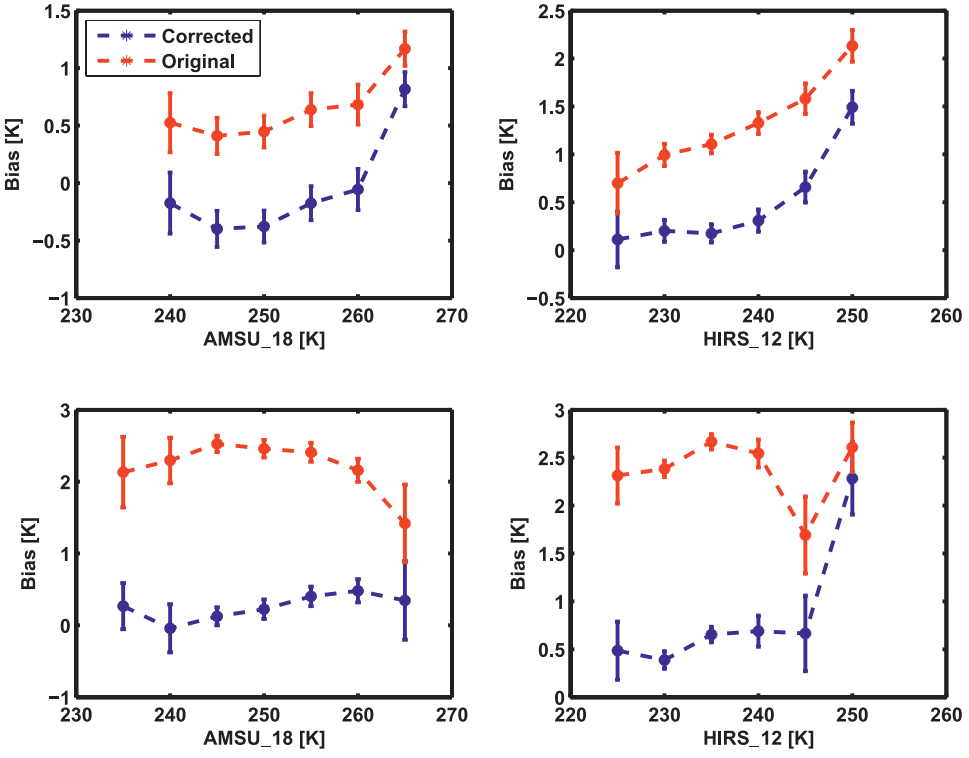

FIG. 3. Bias as a function of brightness temperature binned at 5-K intervals before (red) and after (blue) empirical correction for (left) AMSU-18 and (right) HIRS-12. The standard error (vertical bars), and (top) nighttime and (bottom) daytime data are shown.

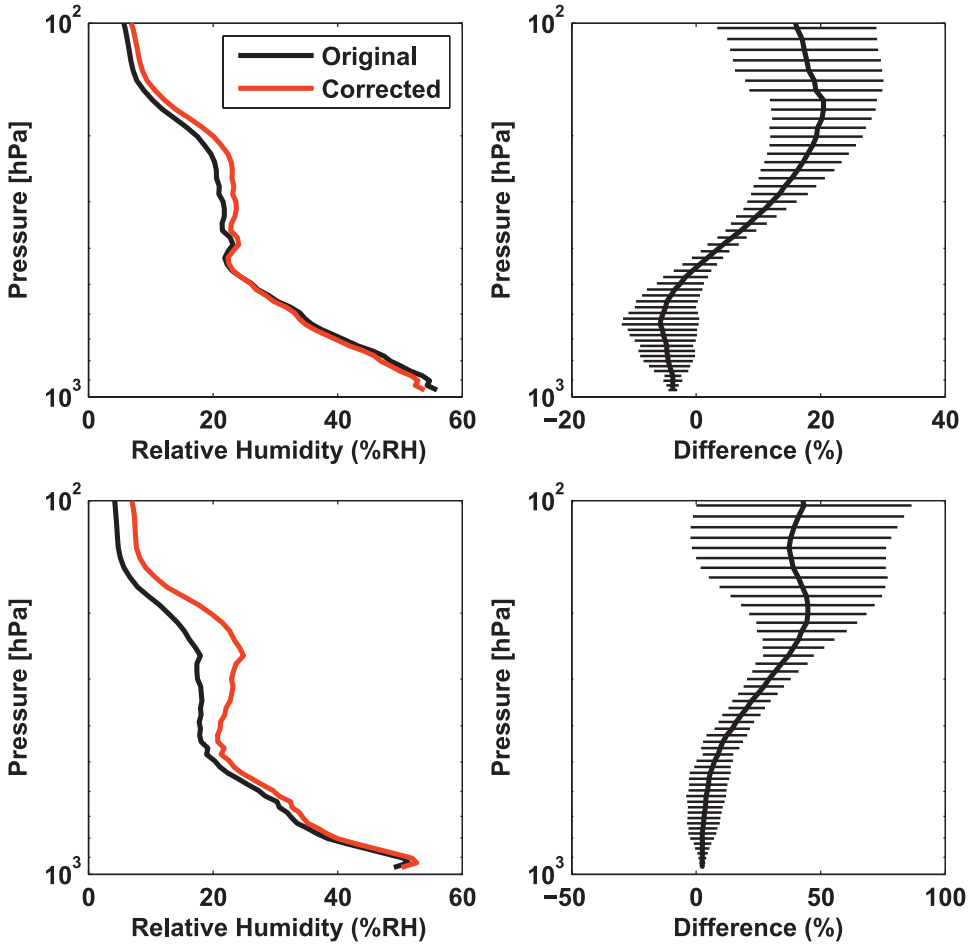

FIG. 4. (left) The mean RH of RS92 radiosonde sensors before (black) and after (red) empirical correction. (right) The mean of the percentage difference between the corrected and the original profiles (thick line), and the standard deviation (horizontal bars) are shown. RH profiles from ARM radiosondes before and after the corrections were interpolated to specific pressure levels (53) ranging from 980 to 100 hPa. The percentage difference is defined as [(corrected−original)/original] × 100%. (top) Nighttime and (bottom) daytime data are shown.

troposphere from wet (low brightness temperature) to dry (high brightness temperature). The impact of empirical correction on the radiosonde profiles themselves can be inferred from Fig. 4, which shows the mean RH of all of the profiles before and after correction. The magnitude of correction is much higher for the daytime data as compared to the nighttime data. It is the solar radiation correction rather than the mean calibration bias correction that accounts for this large difference in the daytime dataset. The bias correction for SRE accounts for more than 50% of the bias reduction in the daytime dataset. It is also worthwhile to mention that the magnitude of the correction is dependent on different humidity conditions in the upper troposphere and is higher under drier conditions for the nighttime dataset, while in the daytime dataset it is higher under moist conditions with the exception of some parts of the upper troposphere (Fig. 5). These results highlight the importance of corrected radiosonde profiles for satellite validation. In addition, the results also reveal that the empirical correction is quite effective in reducing the dry bias of radiosondes in the upper troposphere and leads to a better agreement between HIRS-12 and AMSU-18.

As mentioned earlier, we have used a different algorithm than the published algorithm for mean calibration bias correction. In the nighttime dataset, the correction with the new algorithm results in a bias of 0.35 K in HIRS-12, whereas with the published algorithm it is 0.38 K, but for AMSU-18 these values are −0.07 and −0.10 K, respectively. For the daytime dataset, correction with the new algorithm yields a bias of 1.71 K in HIRS-12 and a bias of 1.75 K with the published

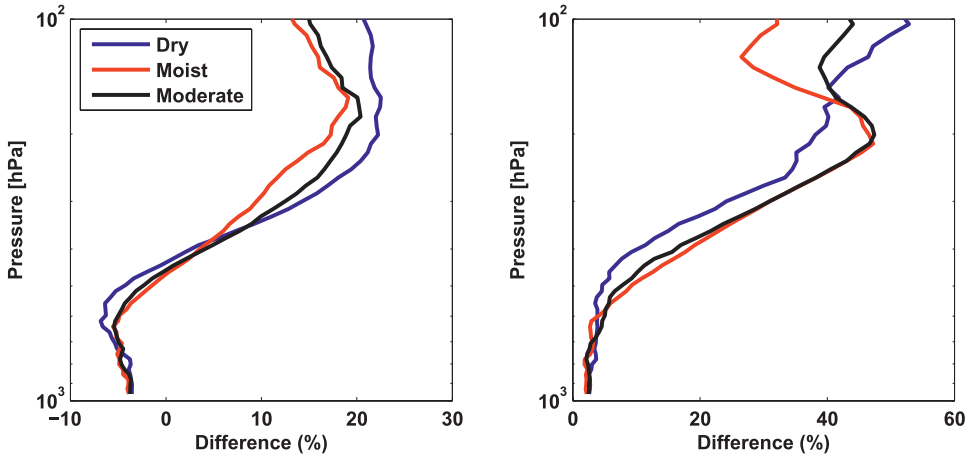

FIG. 5. The percentage difference between the corrected and original profiles classified in terms of different humidity conditions in the upper troposphere (dry, moist, and moderate). Classification is based on the percentiles of the observed brightness temperature in HIRS-12 such that values ≥75 percentile are considered dry, ≤25 percentile are moist, and values ranging between these as moderate. (left) Nighttime and (right) daytime data are shown.

algorithm, while in AMSU-18 these values are 1.76 and 1.78 K, respectively. Although these differences are small, the use of the new algorithm is recommended for mean calibration correction because the temperature dependence is more consistent with actual sensor calibration than the pressure dependence, as used in the published algorithm.

The impact of the TL correction is shown in Table 4. This result reveals that the TL correction has a negligible impact on reducing the bias in AMSU-18 and HIRS-12 because the bias reduction is of the order of only 0.03 K. Because TL correction needs profiles of higher resolution, it is applied here only to a subset of RS92 profiles. A noteworthy observation is that the bias reduction in AMSU-18 and HIRS-12 resulting from empirical correction on this subset is the same as that for all of the RS92 profiles (not shown).

Although the agreement between HIRS-12 and AMSU-18 has been improved because of correction, a small discrepancy of the order of 0.45 K for nighttime and 0.31 K for daytime data still remains. One of the major reasons for the discrepancy can be attributed to the uncertainty in the corrected RS92 measurements. Miloshevich et al. (2009) have shown that the bias uncertainty is ±(4% + 0.5% RH), which implies that 4% of the measured value plus a 0.5% RH offset component is increasingly important for drier conditions. For example, the relative uncertainty in the corrected RS92 data is ±5% for conditions of 50% RH, ±6.5% at 20% RH, ±9% at 10% RH, and ±20% at 3% RH. Therefore, there could be a larger uncertainty in the correction occurring at the HIRS-12 sensing altitude than at the AMSU-18 sensing altitude because it senses a drier atmosphere. A part of the difference could also be attributed to error in the radiative transfer modeling. However, based on the comparison to LBLRTM described in the appendix, we expect this error to be smaller than 0.3 K. Systematic error in the satellite measurements, which is of the order of 0.5 K in AMSU-18 and HIRS-12 on *NOAA-17*, could also play a role (Shi and Bates 2011; John et al. 2012). It is difficult to attribute the remaining discrepancy between AMSU-18 and HIRS-12 to any single cause because it is a very small bias. Therefore, it is only fair to say that the radiosonde, radiative transfer modeling, and systematic error in AMSU/HIRS measurements are equally plausible contributors to the bias.

Coming back to the subject of radiosonde correction, one can state that in addition to significantly reducing the bias between satellite and radiosonde measurements, empirical correction also brings forth a better agreement between AMSU-18 and HIRS-12. The discrepancy in

TABLE 4. Statistics comparing satellite radiance and simulated radiance in brightness temperature units for RS92 sensors. The bias is defined as the mean of simulated minus measured data. SD refers to the standard deviation. The number of profiles used is 85. Suffixes btl and atl refers to before and after time lag correction.

Channel	Bias (K)	Bias in UTH (%)	SD (K)	SD UTH (%)
AMSU-18$_{btl}$	0.14	−0.9	1.52	10.64
AMSU-18$_{atl}$	0.17	−1.2	1.51	10.57
HIRS-12$_{btl}$	0.94	−10.7	1.21	13.80
HIRS-12$_{atl}$	0.91	−10.4	1.19	13.56

the apparent radiosonde bias between HIRS-12 and AMSU-18 before correction in the nighttime dataset was around 10%, and it was lowered to approximately 5% after correction. Similarly, the discrepancy in the uncorrected daytime dataset was 12%, which reduces to 4.7% after correction. These results show that the radiosonde correction is very important in bringing about a better agreement between satellite and radiosonde measurements of UTH.

There have been a number of earlier correction methods for improving the accuracy of RS80 radiosonde sensors (Turner et al. 2003; Miloshevich et al. 2001). However, Soden et al. (2004) showed that these correction procedures offer only a small improvement in the upper troposphere, although they are effective in the lower troposphere. In contrast to this, our work for the RS92 sensors and the Miloshevich et al. (2009) correction method shows a significant improvement, particularly, in the upper troposphere. The present study therefore may open up the possibility of applying a similar correction approach to other radiosonde sensors.

4. Summary and conclusions

The present study evaluates the importance of radiosonde correction in improving the agreement between satellite- and radiosonde-measured UTH. The satellite measurements from infrared (HIRS-12) and microwave (AMSU-18) instruments were used for this purpose. The satellite measurements were collocated with ARM radiosonde profiles. The satellite–radiosonde comparison was performed by simulating the radiances from collocated radiosonde profiles using ARTS. The comparisons were performed only for clear-sky conditions. The empirical correction procedure applied to RS92 radiosonde sensors was found to have a significant impact in reducing the bias in AMSU-18 and HIRS-12. The nighttime bias in AMSU-18 (from 0.63 to −0.10 K) was reduced by 0.73 and by 0.91 K in HIRS-12 (from 1.26 to 0.35 K). During daytime, the decrease in bias is significantly higher, with a reduction of 2.1 K (from 2.38 to 0.28 K) in AMSU-18 and 1.92 K (from 2.51 to 0.59 K) in HIRS-12. This is on account of the bias removal associated with the solar radiation error. The correction also improved the consistency between AMSU-18 and HIRS-12 and reduced the difference between them by 5% in nighttime and by 7% in daytime datasets.

In addition to showing the importance of radiosonde correction for satellite validation, this study also cautions against the use of uncorrected radiosonde profiles for various water vapor–related studies in the upper troposphere. The need for such corrections is especially due to the imperfect characterization and calibration of the sensor output by the manufacturer. The occurrence of a similar or worse type of imperfection as addressed here for Vaisala radiosondes cannot be ruled out for many other operational radiosondes. In any case, accuracy is one aspect that cannot be ignored or compromised in climate-related studies. The correction method developed by Miloshevich et al. (2009) and implemented in this study is an example as to how these errors can be reduced to a significant extent.

Acknowledgments. The authors are thankful to Lisa Neclos at NOAA for providing access to *NOAA-17* level 1B data. Thanks to the U.S. Department of Energy, Office of Science, Office of Biological and Environmental Research, Climate and Environmental Sciences Division for facilitating the use of radiosonde data obtained from their dedicated Atmospheric Radiation Measurement (ARM) Program. Thanks are also due to the ARTS radiative transfer community. We acknowledge the LBLRTM community for providing the code. Special thanks to Eli Mlawer, Oliver Lemke, and Isaac Moradi. Viju John has been supported by the U.K. Joint DECC and DEFRA Met Office Hadley Centre Climate Programme GA01101. This work also contributes to COST Action ES604–Water Vapour in the Climate System (WaVaCS). The work of the Kiruna group was funded by Swedish Space Board, ''Satellite Atmospheric Science'' grant. We thank our three anonymous reviewers for their useful comments that have resulted in improving the content and quality of the paper.

APPENDIX

Model Intercomparison

This is a comparison of results from the ARTS and LBLRTM forward radiance models. LBLRTM (Clough et al. 2005) has been validated against atmospheric radiance spectra from the ultraviolet to the submillimeter wavelength range (Turner et al. 2004). In this study infrared radiances were simulated using LBLRTM version 11.6, which uses the modified water vapor continuum model MT_CKD_2.4. We verified that continuum changes are negligible in the frequency range where HIRS-12 is located, because ARTS uses MT_CKD_1.0 as the continuum model. The line parameters are the same as that for ARTS (HITRAN 2004).

Model intercomparisons were performed for the HIRS water vapor channel (HIRS-12) of *NOAA-14, -15, -16* and *-17*. The simulations were based on a subset of the diverse set of atmospheric profiles from the European Centre for Medium-Range Weather Forecasts

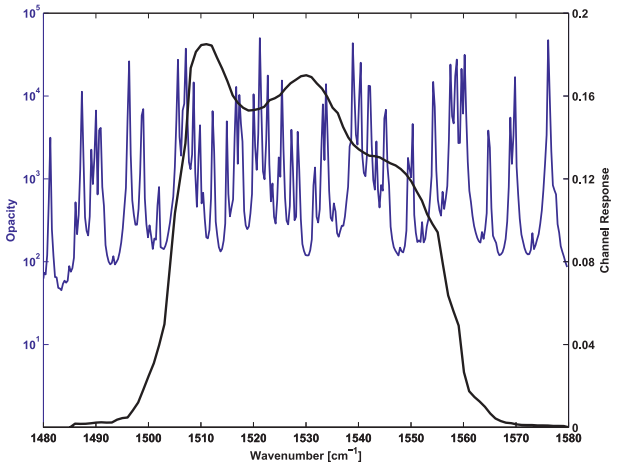

FIG. A1. The H_2O zenith opacity spectrum (blue) and the SRF for HIRS-12 (black) on *NOAA-17*.

(ECMWF) reanalysis data (Chevallier et al. 2006). The number of used profiles is 4700.

Each channel in HIRS has an individual sensor-response function (SRF), specifying the weight as a function of frequency within the spectral range of the channel. The H_2O zenith opacity and the SRF for HIRS-12 is shown in Fig. A1. In the normal line-by-line calculation mode, ARTS simulates the radiances within the pass band of the sensor with a high spectral resolution. These radiances are convolved with the SRF to obtain the radiance of the HIRS channel. For n-frequency grid points within the pass band of the jth HIRS channel, the convolved radiance $R(j)$ is given by

$$R(j) = \frac{\sum_{i=1}^{n} w_i r_i}{\sum_{i=1}^{n} w_i}, \qquad \text{(A1)}$$

where r_i is the radiance for the ith frequency grid point and w_i is the associated weight. The weights for the high-resolution frequency grids are obtained through interpolation from the sensor-specified weights defined for the frequencies within the SRF. However, the fast setup for HIRS in ARTS uses only a few frequencies to simulate the entire HIRS channel radiance. These representative frequencies are selected using a simulated annealing method (Buehler et al. 2010). In the fast setup for HIRS simulations, the weights for $R(j)$ are derived using multiple linear regression over a set of line-by-line calculations using an ensemble of atmospheric conditions.

LBLRTM generates monochromatic infrared radiances with high spectral resolution for a user-specified frequency range. It has no built-in option to consider the SRF or other instrumental properties. Thus, to allow comparison with ARTS, the HIRS channel radiances have been generated by convolving the high-resolution spectra with the respective SRF. The Planck function is used for the conversion of convolved radiance to brightness temperature. During the conversions, care was taken to ensure that the transformations were applied to both of the models in the same manner. Simulations were performed assuming clear-sky conditions and nadir-viewing geometry with a surface emissivity of 1. The statistics of comparison for different NOAA satellites sensors are summarized in Table A1.

TABLE A1. Statistics comparing ARTS and LBLRTM simulations. The bias is defined as the mean of the difference ARTS minus LBLRTM. SD refers to the standard deviation.

Satellite	Channel	Bias (K)	SD (K)
NOAA-14	HIRS-12	−0.07	0.15
NOAA-15	HIRS-12	−0.21	0.23
NOAA-16	HIRS-12	−0.17	0.22
NOAA-17	HIRS-12	−0.21	0.22

REFERENCES

Buehler, S. A., and V. O. John, 2005: A simple method to relate microwave radiances to upper tropospheric humidity. *J. Geophys. Res.,* **110,** D02110, doi:10.1029/2004JD005111.

——, M. Kuvatov, V. O. John, U. Leiterer, and H. Dier, 2004: Comparison of microwave satellite humidity data and radiosonde profiles: A case study. *J. Geophys. Res.,* **109,** D13103, doi:10.1029/2004JD004605.

——, P. Eriksson, T. Kuhn, A. von Engeln, and C. Verdes, 2005: ARTS, the atmospheric radiative transfer simulator. *J. Quant. Spectrosc. Radiat. Transfer,* **91,** 65–93, doi:10.1016/j.jqsrt.2004.05.051.

——, M. Kuvatov, V. O. John, M. Milz, B. J. Soden, D. L. Jackson, and J. Notholt, 2008: An upper tropospheric humidity data set from operational satellite microwave data. *J. Geophys. Res.,* **113,** D14110, doi:10.1029/2007JD009314.

——, V. O. John, A. Kottayil, M. Milz, and P. Eriksson, 2010: Efficient radiative transfer simulations for a broadband infrared radiometer—Combining a weighted mean of representative frequencies approach with frequency selection by simulated annealing. *J. Quant. Spectrosc. Radiat. Transf.,* **111,** 602–615, doi:10.1016/j.jqsrt.2009.10.018.

Chevallier, F., S. Di Michele, and A. P. McNally, 2006: Diverse profile datasets from the ECMWF 91-level short-range forecasts. NWP SAF Satellite Application Facility for Numerical Weather Prediction Doc. NWPSAF-EC-TR-010, version 1.0, 16 pp. [Available online at http://research.metoffice.gov.uk/research/interproj/nwpsaf/rtm/profiles_91L.pdf.]

Clough, S. A., and Coauthors, 2005: Atmospheric radiative transfer modeling: A summary of the AER codes. *J. Quant. Spectrosc. Radiat. Transfer,* **91,** 233–244, doi:10.1016/j.jqsrt.2004.05.058.

Davis, C., C. Emde, and R. Harwood, 2005: A 3D polarized reversed Monte Carlo radiative transfer model for millimeter and submillimeter passive remote sensing in cloudy atmospheres. *IEEE Trans. Geosci. Remote Sens.,* **43,** 1096–1101, doi:10.1109/TGRS.2004.837505.

Deuber, B., J. Morland, L. Martin, and N. Kämpfer, 2005: Deriving the tropospheric integrated water vapor from tipping curve-derived opacity near 22 GHz. *Radio Sci.,* **40,** RS5011, doi:10.1029/2007RG000233.

Elliott, W. P., and D. J. Gaffen, 1991: On the utility of radiosonde humidity archives for climate studies. *Bull. Amer. Meteor. Soc.,* **72,** 1507–1520.

Emde, C., S. Buehler, C. Davis, P. Eriksson, T. Sreerekha, and C. Teichmann, 2004: A polarized discrete ordinate scattering model for simulations of limb and nadir long-wave measurements in 1-D/3-D spherical atmospheres. *J. Geophys. Res.,* **109,** D24207, doi:10.1029/2004JD005140.

Eriksson, P., C. Jiménez, D. Murtagh, G. Elgered, T. Kuhn, and S. Bühler, 2003: Measurement of tropospheric/stratospheric transmission at 10–35 GHz for H_2O retrieval in low Earth orbiting satellite links. *Radio Sci.,* **38,** 8069, doi:10.1029/2002RS002638.

——, S. A. Buehler, C. P. Davis, C. Emde, and O. Lemke, 2011: ARTS, the atmospheric radiative transfer simulator, version 2. *J. Quant. Spectrosc. Radiat. Transfer,* **112,** 1551–1558, doi:10.1016/j.jqsrt.2011.03.001.

Fiorucci, I., and Coauthors, 2008: Measurements of low amounts of precipitable water vapor by millimeter wave spectroscopy: An intercomparison with radiosonde, Raman lidar, and Fourier transform infrared data. *J. Geophys. Res.,* **113,** D14314, doi:10.1029/2008JD009831.

Garand, L., and Coauthors, 2001: Radiance and Jacobian intercomparison of radiative transfer models applied to HIRS and AMSU channels. *J. Geophys. Res.,* **106** (D20), 24 017–24 031.

Held, I. M., and B. J. Soden, 2000: Water vapor feedback and global warming. *Annu. Rev. Energy Environ.,* **25,** 441–475.

John, V. O., and S. A. Buehler, 2004: The impact of ozone lines on AMSU-B radiances. *Geophys. Res. Lett.,* **31,** L21108, doi:10.1029/2004GL021214.

——, and ——, 2005: Comparison of microwave satellite humidity data and radiosonde profiles: A survey of European stations. *Atmos. Chem. Phys.,* **5,** 1843–1853.

——, and B. J. Soden, 2007: Temperature and humidity biases in global climate models and their impact on climate feedbacks. *Geophys. Res. Lett.,* **34,** L18704, doi:10.1029/2007GL030429.

——, G. Holl, S. A. Buehler, B. Candy, R. W. Saunders, and D. E. Parker, 2012: Understanding inter-satellite biases of microwave humidity sounders using global SNOs. *J. Geophys. Res.,* doi:10.1029/2011JD016349, in press.

Kiehl, J. T., and B. P. Briegleb, 1992: Comparison of the observed and calculated clear sky greenhouse implications for climate studies. *J. Geophys. Res.,* **97,** 10 037–10 049.

McMillin, L. M., and C. Dean, 1982: Evaluation of a new operational technique for producing clear radiances. *J. Appl. Meteor.,* **21,** 1005–1014.

Melsheimer, C., and Coauthors, 2005: Intercomparison of general purpose clear sky atmospheric radiative transfer models for the millimeter/submillimeter spectral range. *Radio Sci.,* **40,** RS1007, doi:10.1029/2004RS003110.

Miloshevich, L. M., H. Vömel, A. Paukkunen, A. J. Heymsfield, and S. J. Oltmans, 2001: Characterization and correction of relative humidity measurements from Vaisala RS80-A radiosondes at cold temperatures. *J. Atmos. Oceanic Technol.,* **18,** 135–156.

——, A. Paukkunen, H. Vömel, and S. J. Oltmans, 2004: Development and validation of a time-lag correction for Vaisala radiosonde humidity measurement. *J. Atmos. Oceanic Technol.,* **21,** 1305–1327.

——, H. Vömel, D. N. Whiteman, and T. Leblanc, 2009: Accuracy assessment and correction of Vaisala RS92 radiosonde water vapor measurements. *J. Geophys. Res.,* **114,** D11305, doi:10.1029/2008JD011565.

Mlawer, E. J., S. A. Clough, and D. C. Tobin, 2003: A new water vapor continuum model: MT_CKD_1.0. *Proc. ARM Science Team Meeting,* ARM, Broomsfield, CO. [Available online at http://www.arm.gov/publications/proceedings/conf13/poster_abs/P00225.]

Moradi, I., S. A. Buehler, V. O. John, and S. Eliasson, 2010: Comparing upper tropospheric humidity data from microwave satellite instruments and tropical radiosondes. *J. Geophys. Res.,* **115,** D24310, doi:10.1029/2010JD013962.

Rosenkranz, P. W., 1993: Absorption of microwaves by atmospheric gases. *Atmospheric Remote Sensing by Microwave Radiometry,* M. A. Janssen, Ed., John Wiley and Sons, 37–90.

——, 1998: Water vapor microwave continuum absorption: A comparison of measurements and models. *Radio Sci.,* **33,** 919–928; Corrigendum, **34,** 1025.

Rothman, L. S., and Coauthors, 2003: The HITRAN molecular spectroscopic database: Edition of 2000 including updates through 2001. *J. Quant. Spectrosc. Radiat. Transfer,* **82,** 5–44.

Saunders, R., and Coauthors, 2007: A comparison of radiative transfer models for simulating Atmospheric Infrared Sounder (AIRS) radiances. *J. Geophys. Res.,* **112,** D01S90, doi:10.1029/2006JD007088.

Shi, L., and J. J. Bates, 2011: Three decades of intersatellite-calibrated High-Resolution Infrared Radiation Sounder upper tropospheric water vapor. *J. Geophys. Res.,* **116,** D04108, doi:10.1029/2010JD014847.

Soden, B. J., and F. P. Bretherton, 1993: Upper tropospheric relative humidity from the GOES 6.7 μm channel: Method and climatology for July 1987. *J. Geophys. Res.,* **98** (D9), 16 669–16 688.

——, and J. R. Lanzante, 1996: An assessment of satellite and radiosonde climatologies of upper-tropospheric water vapor. *J. Climate,* **9,** 1235–1250.

——, D. D. Turner, B. M. Lesht, and L. M. Miloshevich, 2004: An analysis of satellite, radiosonde, and lidar observations of upper tropospheric water vapor from the Atmospheric Radiation Measurement Program. *J. Geophys. Res.,* **109,** D04105, doi:10.1029/2003JD003828.

Turner, D. D., B. M. Lesht, S. A. Clough, J. C. Liljegren, H. E. Revercomb, and D. C. Tobin, 2003: Dry bias and variability in Vaisala RS80-H radiosondes: The ARM experience. *J. Atmos. Oceanic Technol.,* **20,** 117–132.

——, and Coauthors, 2004: The QME AERI LBLRTM: A closure experiment for downwelling high spectral resolution infrared radiance. *J. Atmos. Sci.,* **61,** 2657–2675.

Vömel, H., D. E. David, and K. Smith, 2007a: Accuracy of tropospheric and stratospheric water vapor measurements by the cryogenic frost point hygrometer: Instrumental details and observations. *J. Geophys. Res.,* **112,** 1–14.

——, and Coauthors, 2007b: Radiation dry bias of the Vaisala RS92 humidity sensor. *J. Atmos. Oceanic Technol.,* **24,** 953–963.